## Multiple data sets converge on a geologic structural model for Glass Buttes, Oregon geothermal prospect

## ORMAT<sup>®</sup>

Geologic field work is being combined with multiple remote sensing and geophysical

Oregon. Glass Buttes are a Pliocene volcanic center that sits near the junction of the

Abert Rim and Brothers Fault Zones. West-northwest-striking faults, which typify the

Brothers Fault Zone, bound Glass Buttes. Individual faults and fault intersections are

anticipated to provide permeability for utility scale geothermal development in central

Oregon. Existing temperature data reveal a maximum of 90° C measured at 600 m,

with ~160° C/km bottom hole temperature gradient. High temperature surface altera-

tion, abundant WNW-oriented faulting, and reported drilling mud losses indicate likely

commercial temperatures and fracture-controlled permeability at depth. LiDAR, hyper-

spectral mineral mapping, and field mapping constrain near-surface structure and vol-

canic contacts; aeromagnetic data constrain surface to intermediate (<1000 m) struc-

ture; and gravity data constrain deeper structure (surface-2000 m). Data sets agree

reasonably well in some areas, although gravity data reflect a few deep-seated faults

these interpreted faults trend ENE, nearly perpendicular to observed surface struc-

tures. To the north of Glass Buttes, a curvilinear gravity high and topographic low indi-

cate that Glass Buttes sits on the southern end of a previously unidentified buried cal-

dera or graben. Interpretation of subsurface and gravity data do not uniquely distin-

guish between these alternative interpretations. Exploratory drilling will target inter-

sections of surface faults with deeper gravity-defined features.

more than the densely faulted surface structure. On the east side of the prospect,

tools to model fault structure at the Glass Buttes geothermal prospect in central

Abstract

Patrick Walsh<sup>1</sup>, Brigette A. Martini<sup>1</sup>, Chet Lide<sup>2</sup>, Darrick Boschmann<sup>3</sup>, John Dilles<sup>3</sup>, and Andrew Meigs<sup>3</sup>

<sup>1</sup>Ormat Nevada, Inc.; <sup>2</sup>Zonge Geosciences; <sup>3</sup>Oregon State University

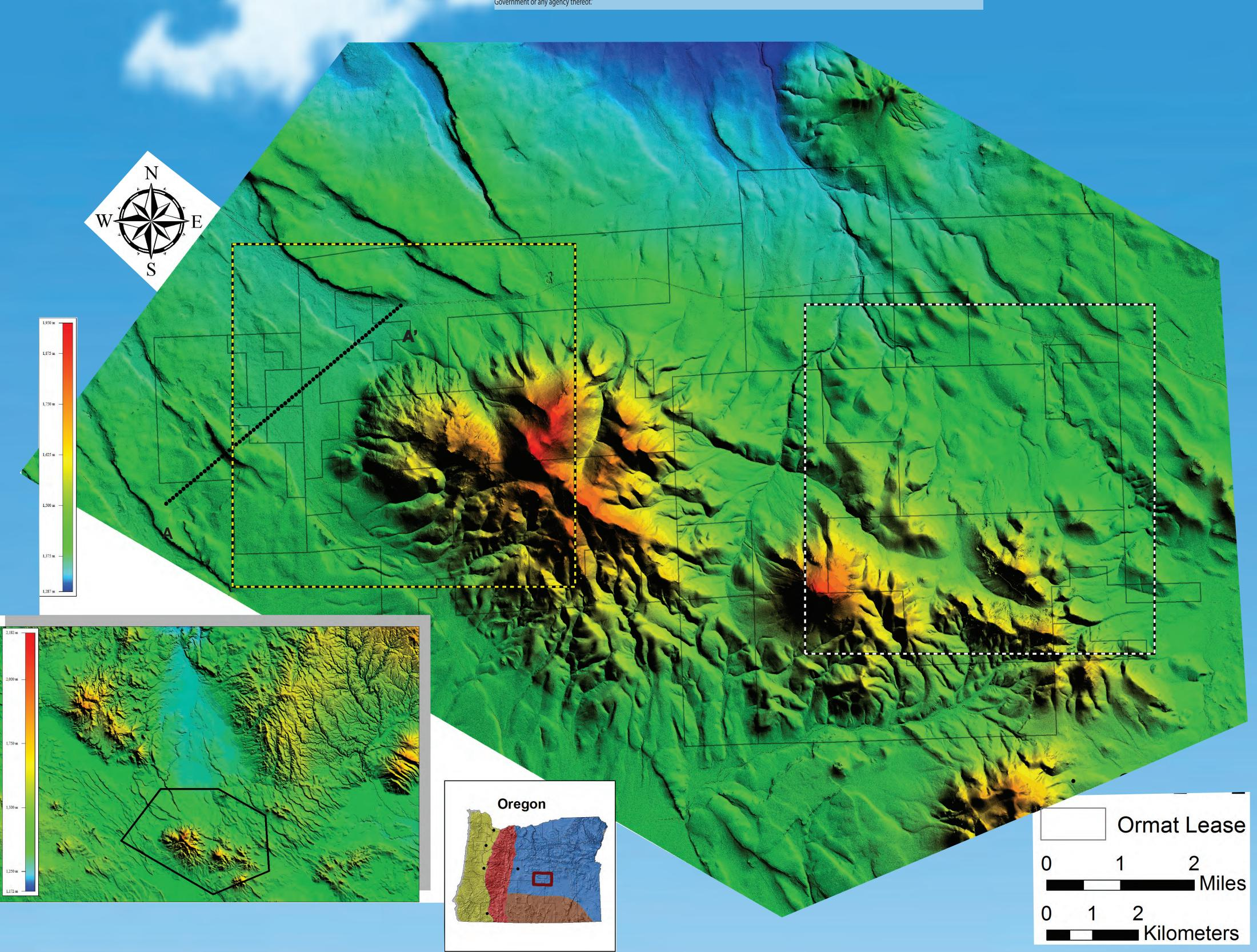
## pwalsh@ormat.com



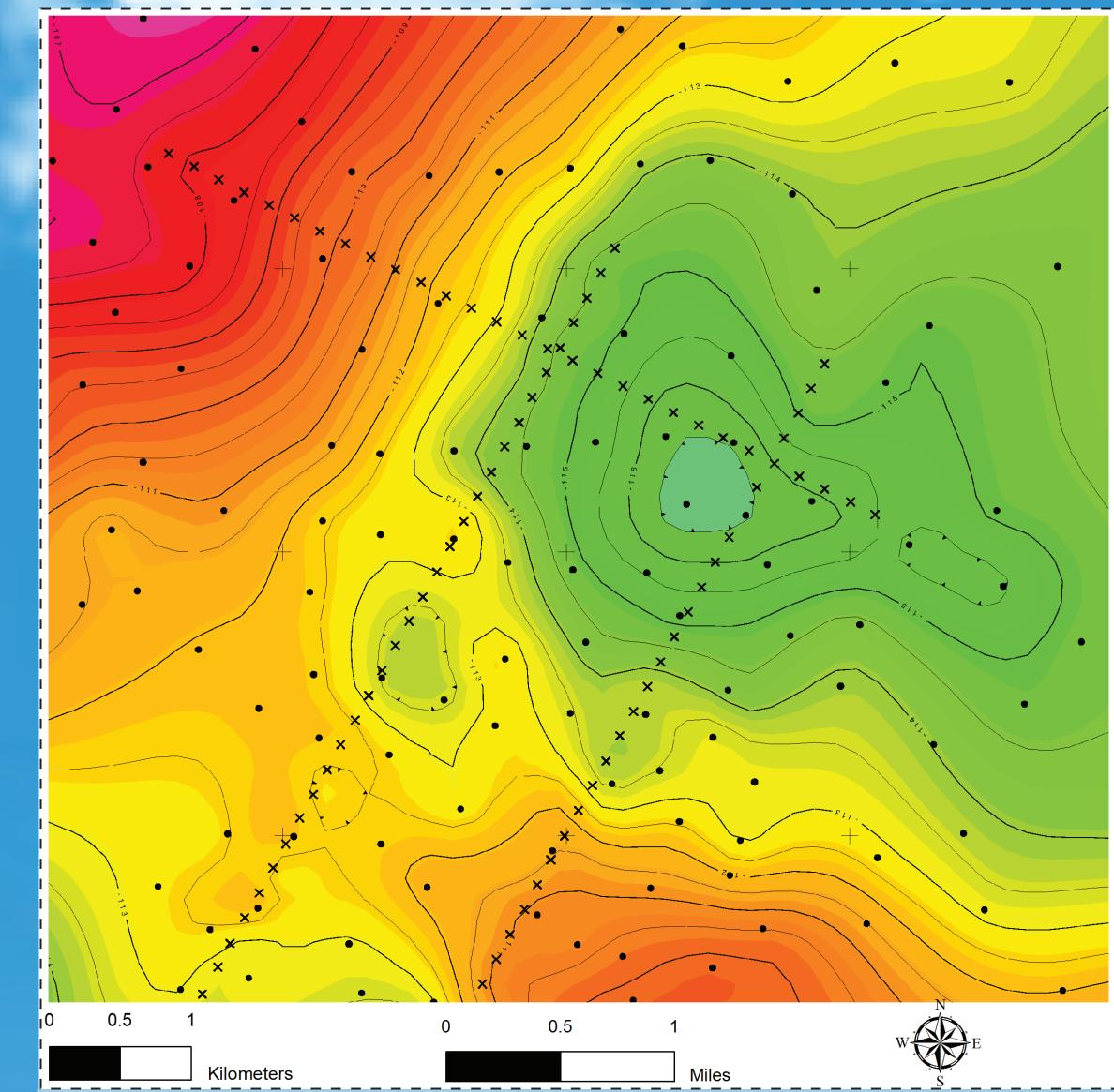




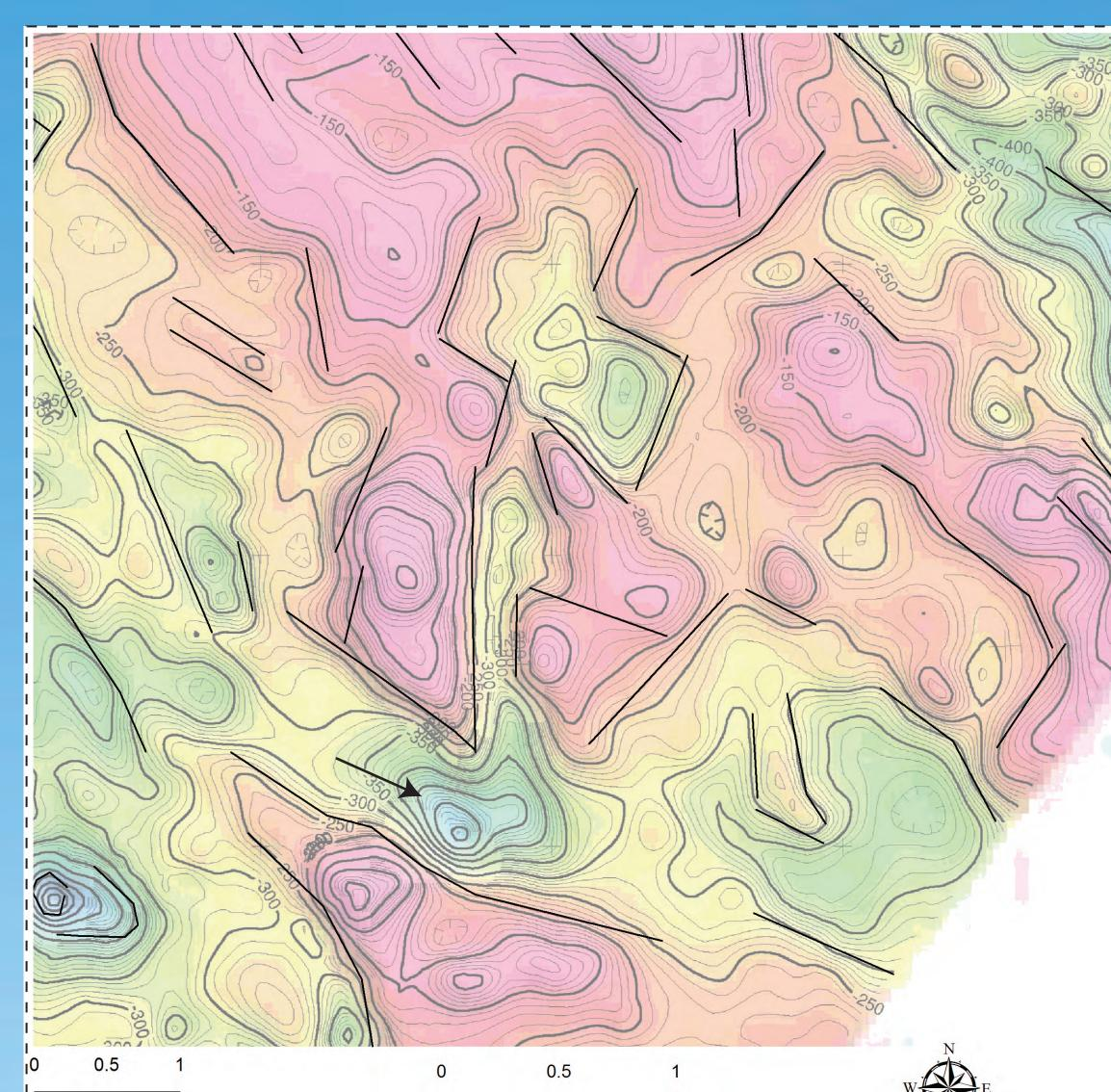
Disclaimer: "This report was prepared as an account of work sponsored by an agency of the United States Government. Neither the United States Government nor any agency thereof, nor any of their employees, makes any warranty, express or implied, or assumes any legal liability or responsibility for the accuracy, completeness, or usefulness of any information, apparatus, product, or process disclosed, or represents that its use would not infringe privately owned rights. Reference herein to any specific commercial product, process, or service by trade name, trademark, manufacturer, or otherwise does not necessarily constitute or imply its endorsement, recommendation, or favoring by the United States Government or any agency thereof. The views and opinions of authors expressed herein do not necessarily state or reflect those of the United States



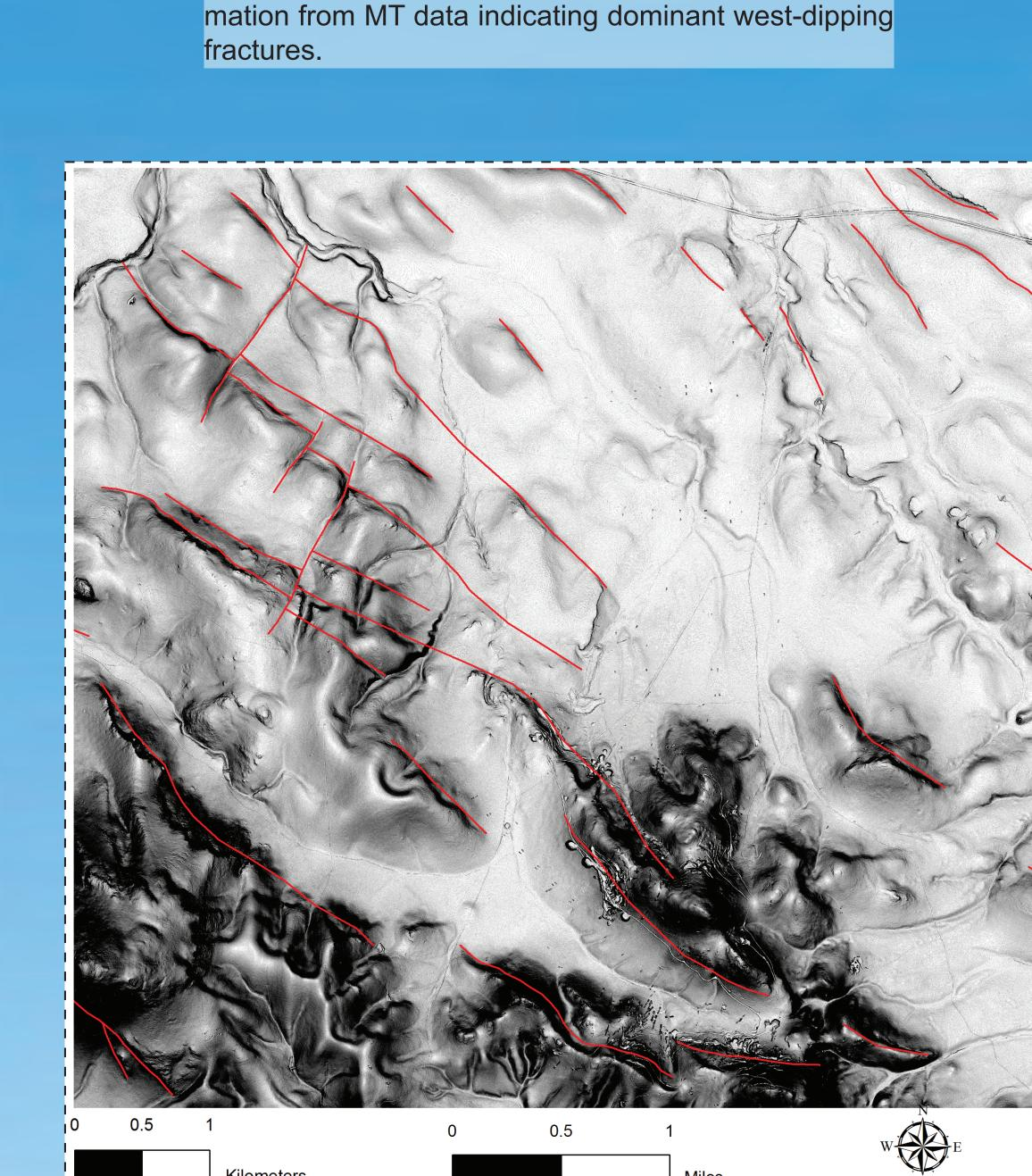
Digital elevation model (DEM) with shaded relief. Dashed boxes outline areas of detail for the rest of the poster. All figures to the right correspond with the same area and scale as the eastern box; all images to the left correlate with the western box. Large inset map includes shaded relief DEM from US NED 30 m and outline of LiDAR data displayed in main figure. Small inset includes physiographic provinces of Oregon(USGU) and outline of large inset. Physiographic provinces include Pacific border (yellow), Cascade-Sierra Mountains (red), Basin and Range (brown), and Columbia Plateau (Blue).



Bouger gravity calculated with a reduction density of 2.35 gm/cc over eastern dashed area shown on DEM map. Black dots and x's mark station locations. Contour interval is 0.5 mgal. Intersection of NNE-trending and ESE-trending structure may provide fluid conduit. Gravity low in northeast area would typically be interpreted as downthrown to both faults, in contrast with results from MT data.



Reduced to pole aeromagnetic data with lineament interpretation. Several apparent structures correlate with faults mapped from LiDAR or on the surface (image to the right). Low magnetic susceptibility in the southeast correlates with area of hydrothermal alteration (e.g. hyperspectral image below left). The area of lowermagnetic susceptibility indicated by the arrow may indicate buried alteration.

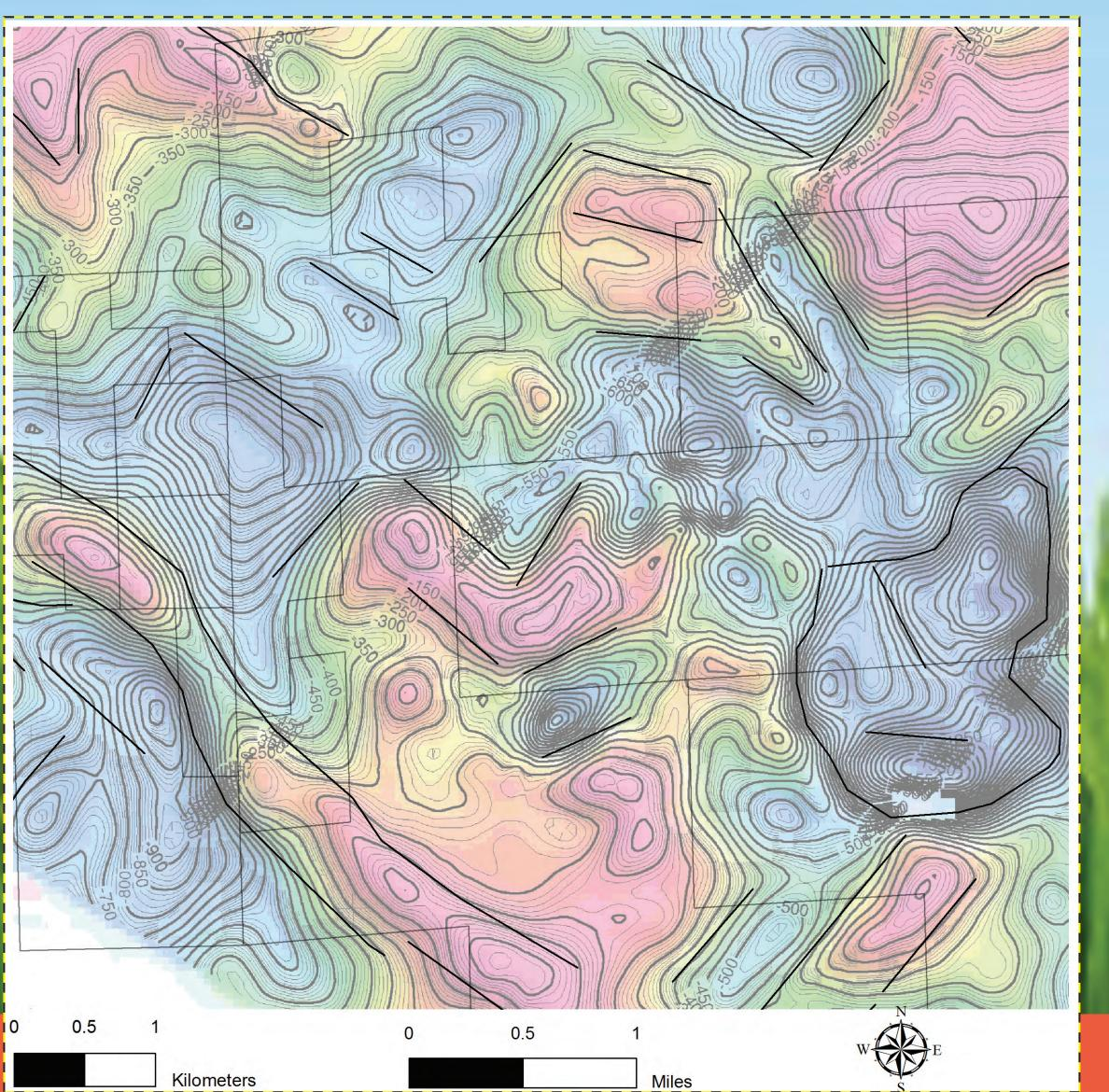


Preliminary density models illustrate amiguity in gravity

data. These models will be recreated following infor-

Glass Buttes Profile 4, V2

Slope-shade map of LiDAR data with mapped faults (red). High slopes in black, low slopes in white. Note extensive mining disturbance feeatures in the southcentral portion of the image.

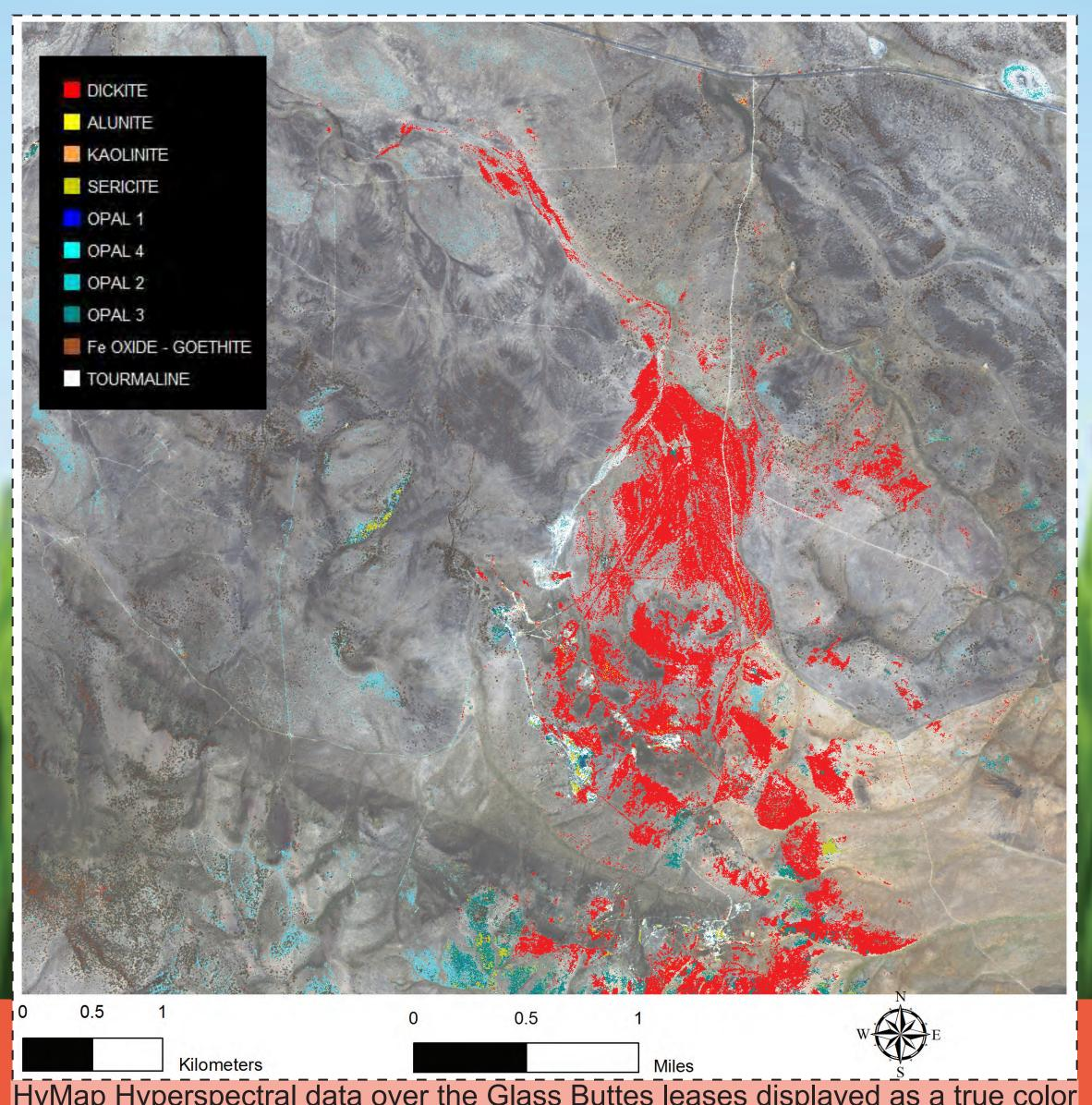


Reduced to pole aeromagnetic data with lineament interpretation.

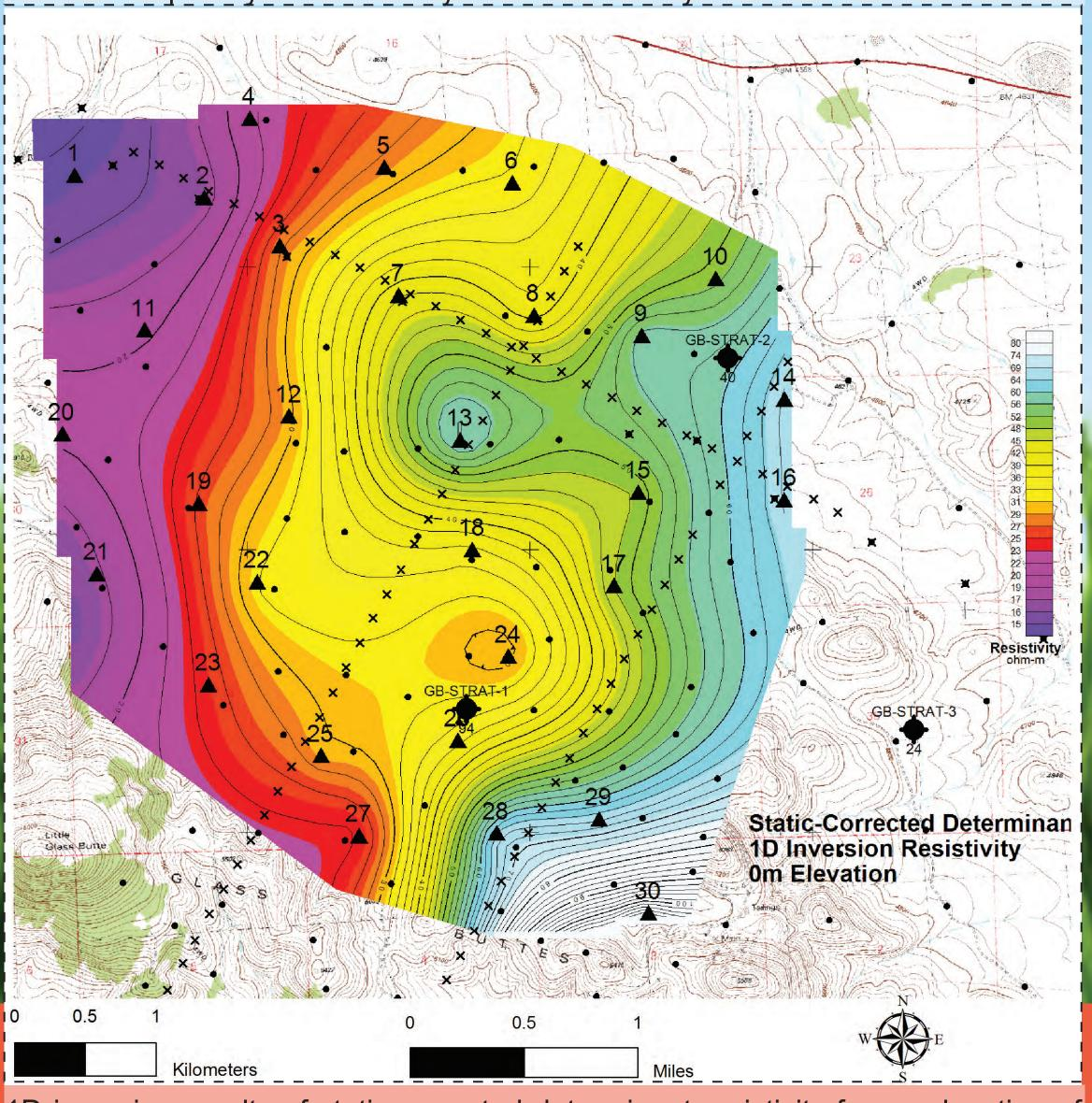
low slopes in white. Glass Butte is the high relief area on the east side of the map. tions)

Parmele Ridge Fault is the prominant feature on the southwest side of the map.

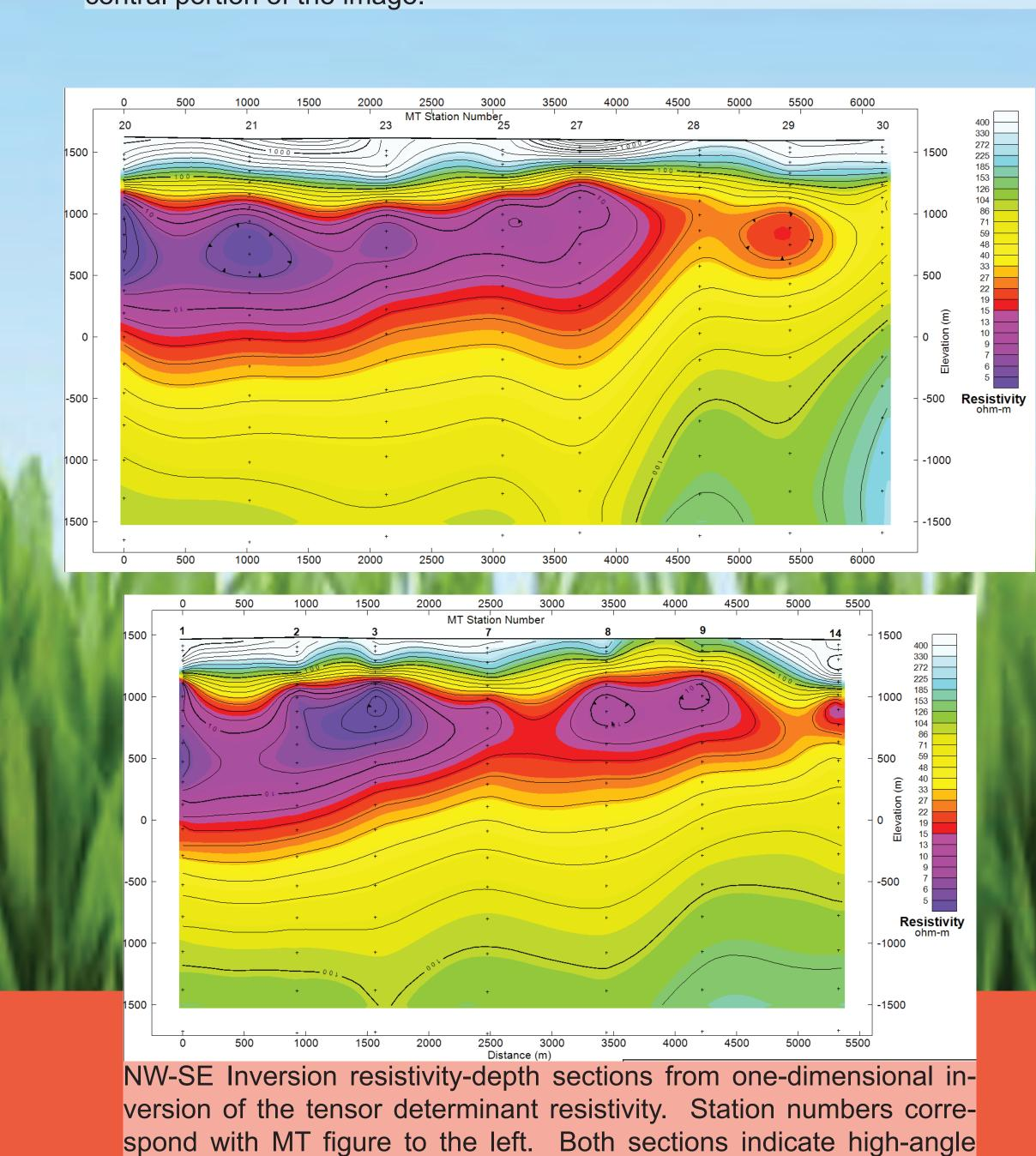
Slope-shade map of LiDAR data with mapped faults (red). High slopes in black, (Johnson and Ciancanelli, 1983, GRC Transac-



HyMap Hyperspectral data over the Glass Buttes leases displayed as a true color image. Extremely bright, disturbed areas will appear white to light blue/cyan. Overlay pixels colored according to mineralization described in inset legend. Classification from full spectral unmixing algorithms.



1D inversion results of static-corrected determinant resistivity for an elevation of 0 m, or approximate target depth for first slim well. North-south gradient is likely to be high angle faulting, as shown on sections to the right.



down to the west faulting.

Time... The Only True Test of Reliability Overlay pixels colored accompanies. The Only True Test of Reliability Sification from full spectral of the Colored accompanies.

SW-NE Inversion resistivity-depth section from

nant resistivity. Location indicated by A-A' on

80 100 120 140 160 180 200

one-dimensional inversion of the tensor determi-